Journal of Nuclear Materials 405 (2010) 181–185

Contents lists available at ScienceDirect

Journal of Nuclear Materials

journal homepage: www.elsevier.com/locate/jnucmat

Deuterated target comparison for pyroelectric crystal D–D nuclear fusion experiments

Donald J. Gillich [a], Andrew Kovanen [a], Yaron Danon [b,*]

[a] Department of Physics and Nuclear Engineering, United States Military Academy, West Point, NY 10996, United States
[b] Department of Mechanical, Aerospace, and Nuclear Engineering, Rensselaer Polytechnic Institute, Troy, NY 12180, United States

ARTICLE INFO

Article history:
Received 24 March 2010
Accepted 13 August 2010

ABSTRACT

Different target materials were investigated to determine which ones are favorable to increasing the theoretical neutron yield using pyroelectric crystal D–D nuclear fusion. Calculations show that deuterated polyethylene (CD_2) will potentially yield the highest number of neutrons compared to the other targets investigated. However, deuterated plastic targets have been found to erode over the course of experiments.

Published by Elsevier B.V.

1. Introduction

Pyroelectric crystals have been used to achieve D–D nuclear fusion through the ionization of D_2 gas and acceleration of deuterium ions into a deuterated target. Groups at Lawrence Livermore National Laboratory (LLNL) [1] and Rensselaer Polytechnic Institute (RPI) [2–5] have reported using deuterated plastic targets to achieve D–D nuclear fusion using pyroelectric crystals. One focus of the research at RPI is to increase the yield of neutrons generated by D–D fusion closer to the theoretical limit. As part of the research effort, different deuterated targets were investigated to determine which materials were more likely to facilitate greater neutron production.

Pyroelectric crystals have intrinsic dipole moments and exhibit spontaneous polarization, P_s, defined as the dipole moment per unit volume of the material, when heated or cooled [6]. These crystals are usually cut such that a net dipole moment is perpendicular to the flat surfaces, usually named the $-z$ and $+z$ faces. When the temperature is constant (equilibrium conditions), free charged particles assemble at the faces of the crystal to screen the charge due to P_s. As the temperature of the crystal changes, P_s changes and charge moves at the crystal face to compensate for the change in P_s.

Consider a crystal being heated. As P_s decreases the $+z$ face becomes less positive but not fully negative while the $-z$ face becomes less negative but not fully positive until both reach their final charges. Therefore electrons will be attracted towards the initial $-z$ face while positive ions are attracted toward the initial $+z$ face. During cooling, this process is reversed. To reduce frequent crystal discharges, experiments are done under vacuum at low ambient D_2 gas pressure (1–10 mtorr) which reduces the number of charged particles available near the crystal surface.

The change in spontaneous polarization, ΔP_s, is equal to the amount of surface charge on each face of the crystal. ΔP_s can be calculated by multiplying the change in temperature by the pyroelectric coefficient, γ, such that

$$\Delta P_s = \gamma \cdot \Delta T \tag{1}$$

where γ is typically given in $\mu C\ m^{-2}\ K^{-1}$ and ΔT is in K. For $LiTaO_3$ crystals in the temperature range of interest, the value [7] for γ is 190 $\mu C\ m^{-2}\ K^{-1}$. ΔT is about 100 K in typical experiments at RPI. To get the total charge, Q, on the surface of the crystal this value is multiplied by the z face surface area, A, such that

$$Q = \Delta P_s \cdot A \tag{2}$$

For a 15 mm radius cylindrical $LiTaO_3$ crystal, the total charge generated on the crystal surface is 8.4×10^{13} elementary charges (1.3×10^{-5} C) per thermal cycle.

During experiments, acceleration energies are measured using an X-ray detector to observe Bremsstrahlung radiation resulting from energetic electrons interacting with surrounding materials. Because the electrons are interacting with the aluminum and stainless steel flanges and vacuum chamber, a soft X-ray spectrum is expected. The measured Bremsstrahlung end-point energy was assumed to be the maximum accelerating potential influencing the charged particles. Accelerating potentials of 180 kV have been experimentally observed at RPI using a two-crystal system [2].

A calculation of the theoretical neutron production limit was performed for each material of interest to determine which deuterated target materials were likely to attain higher neutron yields. Cross section data was taken from ENDF/B-VII [8] and calculations were completed using the Stopping and Range of Ions in Matter (SRIM 2008) with the Transport of Ions in Matter (TRIM) computer code [9].

* Corresponding author. Tel.: +1 518 276 4008; fax: +1 518 2764832.
E-mail address: danony@rpi.edu (Y. Danon).

0022-3115/$ - see front matter Published by Elsevier B.V.
doi:10.1016/j.jnucmat.2010.08.012

D–D fusion results in one of two possible branches

$$D + D \rightarrow He^3\,(0.82\ \text{MeV}) + n\,(2.45\ \text{MeV})$$
$$D + D \rightarrow T\,(1.01\ \text{MeV}) + H\,(3.02\ \text{MeV})$$

which have about the same probability of occurring over a large range of energies. These reactions are usually called the "neutron branch" and "proton branch" respectively [10]. The cross section for the neutron branch was used to calculate the number of neutrons that may be produced. Fig. 1 is a plot of the neutron branch and D–T fusion reaction cross section data as a function of D^+ energy.

The number of fusions per incident D^+ ion (fusion reaction rate) per distance traveled in the target as a function of depth is given by

$$R(x)dx = \phi_x N_D \sigma(E(x))dx \tag{3}$$

where $R(x)$ is the probability that a fusion will occur per unit length, ϕ_x is the ion current, N_D is the number density of deuterium atoms in the target material (cm^{-3}), $\sigma(E(x))$ is the D–D fusion neutron branch cross section as a function of deuteron energy [barns], and dx is a differential distance along the deuteron travel path [nm]. Eq. (3) assumes that ions are not lost as they penetrate into the target but only lose energy such that the current as a function of depth is constant.

The SRIM Code was used to calculate the energy loss per unit length in the target material, $\frac{dE(x)}{dx}$, as a function of depth. This data was then used to calculate the energy of D^+ ions as a function of depth traveled in the target, x,

$$E(x) = E_0 - \int_0^x \frac{dE(x)}{dx}dx \tag{4}$$

where E_0 is the initial accelerating ion energy (assumed to be 180 keV). Fig. 2 represents a plot of $\frac{dE}{dx}$ and ion energy as a function of depth in the target.

The microscopic cross section for D–D fusion as a function of depth, $\sigma(E(x))$, can then be calculated. Figure gives the graph of cross section versus the depth for a slowing down 180 keV D+ ion. From this figure it can be seen that the fusion cross section approaches zero at around 1.8 μm which means that deuterated polyethylene targets thicker than 1.8 μm are unnecessary. A total integral cross section, σ_{int}, can be calculated by integrating the cross section over the range of the ion in the target material (see Fig. 3):

$$\sigma_{int} = \int_0^{Range} \sigma(E(x))dx \tag{5}$$

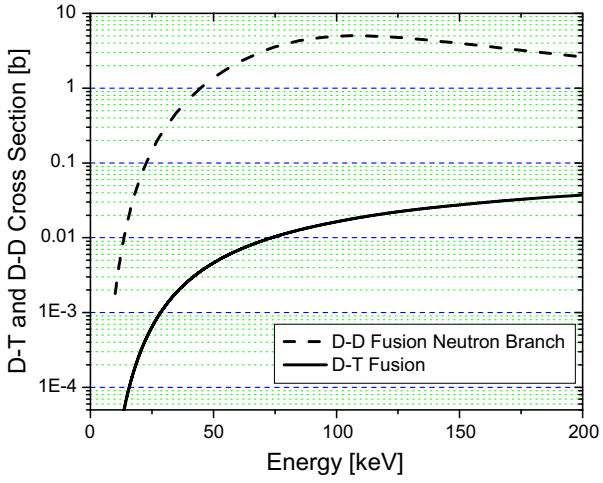

Fig. 1. Neutron branch cross section as a function of D^+ energy.

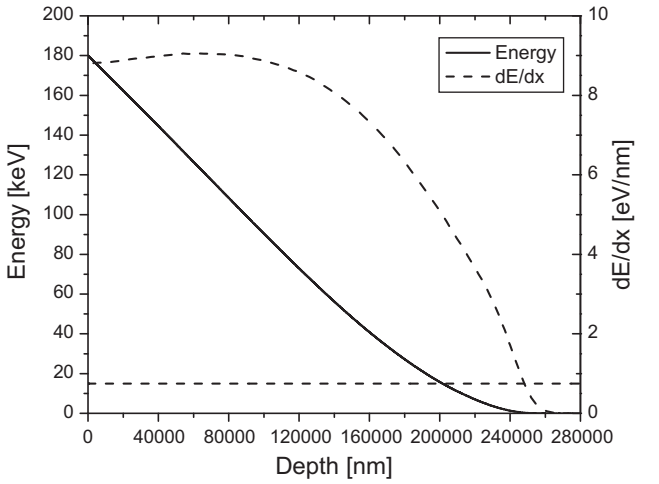

Fig. 2. Graph of energy and $\frac{dE}{dx}$ versus target depth for 180 keV D^+ ions impacting a CD_2 target. The fusion threshold is approximately 15 keV and the ion range is about 2 μm.

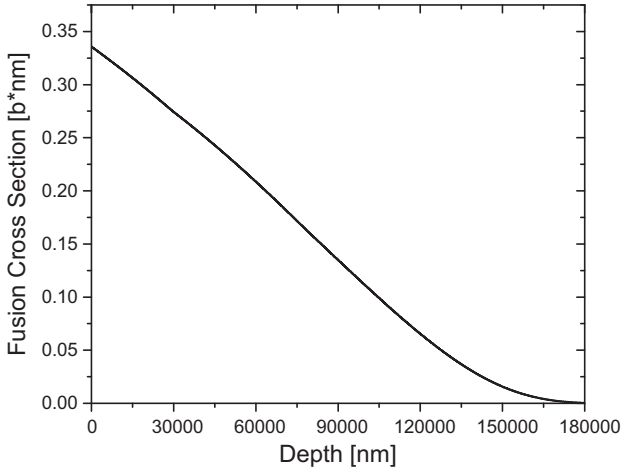

Fig. 3. D–D fusion (neutron branch) cross section as a function of depth for slowing down 180 keV D^+ ions.

The density of deuterium atoms per cm^3 can be calculated using:

$$N_D = \frac{2\rho N_A}{M} \tag{6}$$

where ρ is the target density, N_A is Avogadro's number, and M is the mass of CD_2. The factor of 2 is included because there are two deuterium atoms per carbon.

The theoretical number of neutrons can then be calculated using:

$$S = \int_0^{Range} R(x)dx = \phi_x \cdot N_D \cdot \sigma_{int} \tag{7}$$

where ϕ_x is the ion current as defined in Eq. (3), σ_{int} is the total integrated cross section and N_D is the number density of deuterium atoms in the target.

The fusions per incident ion as a function of depth can be calculated using Eq. (7) and is plotted in Fig. 4. The probability to achieve fusion reaction approaches zero at around 1.8 μm, therefore, even though the range of the 180 keV deuterium ions in CD_2 was estimated to be 2.1 μm, fusion will likely occur only with-

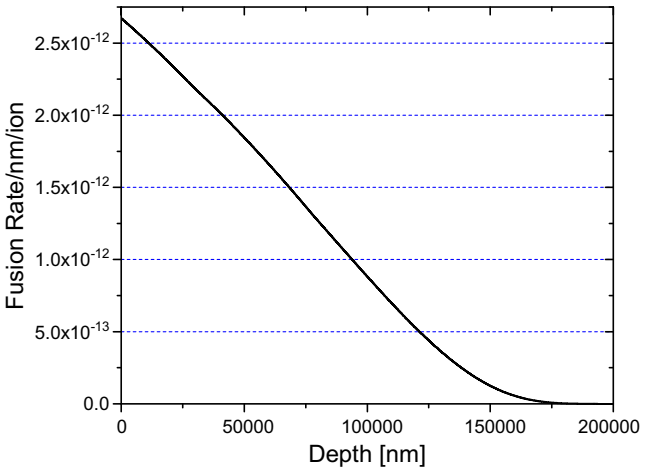

Fig. 4. Neutron branch fusion reaction rate as a function of depth.

in the first 1.8 μm of the target thickness. The depth at which the fusion rate goes to zero in Fig. 4 confirms the D–D fusion energy threshold as shown in Fig. 2.

2. Target comparison calculations

The calculations were based on a 1.5 cm radius crystal with a ΔT of 100 K. It was assumed that every charge generated on the crystal face produced a D^+ ion (100% ionization efficiency) and that these ions experienced an accelerating potential of 180 kV. For the SRIM calculation a deuterated polyethylene (CD_2) target nominal density was assumed to be 1.06 g cm^{-3}. For the CD_2 target the integral cross section was calculated using Eq. (5) to be approximately 2589 b-nm. Using Eq. (6), a deuterium atom density of 4.5×10^{22} cm^{-3} for deuterated polyethylene was calculated.

Based on these assumptions and using the number of electrons from Eq. (2), the number of deuterium ions (D^+) per thermal cycle, φ_x, was 8.4×10^{13} ions resulting in 1.7×10^7 D–D fusion neutrons per thermal cycle. The same calculation using tritium gas and the microscopic cross section for the D–T reaction as shown in Fig. 1 was also performed. Assuming a 120 s emission cycle, the neutron yield increased by a factor of about 210 giving a total theoretical neutron yield of 3.1×10^7 neutrons per second.

Similar calculations were used to investigate other target materials to include: deuterated polystyrene (CD), titanium (TiD_2), zirconium (ZrD_2), yttrium (YD_2), scandium (ScD_2) and erbium (ErD_2) targets. The types of metals that were investigated in this analysis were chosen based on their ability to absorb hydrogen. The composition stoichiometry of a molecule refers to the atomic concentration of constituent elements. For example, TiD_x is a molecule with one titanium atom and x deuterium atoms. While theoretically a 2 to 1 ratio of hydrogen to metal atoms is possible for titanium (i.e. $x = 2$), actual deuterated targets have been found to have less than a 2 to 1 ratio of deuterium to metal atoms [14]. For this comparison, the theoretical limit (2 to 1 ratio) was used for the calculations presented here.

An energetic D^+ ion will travel a longer distance in target material that has a low Z number and low number density because the linear stopping power will be lower than a high Z, high density material. As a result, the integrated D–D fusion cross section, $\sigma_{int}(E(x))$, is expected to be higher for low Z, low density materials and therefore, a higher neutron yield would be expected. Also, although a higher density results in higher deuterium density and thus higher fusion rate, the reaction is actually dominated by the stopping power. The deuterated material densities that were used as an input to TRIM were obtained by looking up the material density of each metal hydride in various references as presented in Table 1. To account for deuterium instead of hydrogen atoms, a ratio of the densities compared with the mass of the hydrogenated and deuterated metals was taken. The following equation was used:

$$\rho_{\mathrm{metalD_2}} = \frac{M_{\mathrm{metalD_2}}}{M_{\mathrm{metalH_2}}}\rho_{\mathrm{metalH_2}} \tag{8}$$

where $\rho_{\mathrm{metalD_2}}$ and $\rho_{\mathrm{metalH_2}}$ are the physical densities and $M_{\mathrm{metalD_2}}$ and $M_{\mathrm{metalH_2}}$ are the atomic masses of the deuterated and hydrogenated metals respectively. Table 1 provides a list of the densities used as input to the TRIM calculations.

The ion distribution and quick calculation function in TRIM was used to calculate projected range data. The angle of incidence was assumed to be 0° and the number of ions was set at 1×10^4 to ensure good counting statistics. Table 1 shows ion range values as calculated by TRIM. The code also provided the linear stopping power, $\frac{dE}{dx}$, which was used to calculate the theoretical neutron limit as described above.

When calculating the projected range, higher density materials were found to have a larger amount of straggling (lateral and longitudinal spread of ions). Pyroelectric targets are large (usually 2–3 cm in diameter) compared to these straggling distances (on the order of tenths of microns). Therefore, it was assumed that this density effect was negligible.

3. Experimental results using CD_2

The deuterated polyethylene (CD_2) targets used in the experiments at RPI were made by melting CD_2 in xylene, dropping the liquid plastic onto the surface of the crystal and allowing the plastic to cool. Deuterated polystyrene (CD) targets have been used previously in pyroelectric fusion experiments [1,2]. Deuterated metal targets are usually manufactured by heating the metal to high temperatures (~400 °C, material dependent) in a vacuum to outgas the material. Deuterium gas is then introduced into the vacuum chamber (at a pressure of 3×10^2–10^4 Pa) and the metal is allowed to cool [15]. The metal acts like a sponge by absorbing hydrogen through a diffusive process as it cools; whereby, the hydrogen atoms diffuse into interstitials of the metal lattice [16,17].

Table 1
Target materials comparison.

Material	Hydrogenated density [11–14] (g/cm^3)	Deuterated density (g/cm^3)	Projected range (nm)	Integrated cross section (barn-nm)	Theoretical neutron yield
CD_2 (polyethylene)	0.93	1.06	211,000	2589	1.73E+07
CD (polystyrene)	1.06	1.14	215,000	2639	1.08E+07
TiD_2	3.75	3.90	109,000	1395	1.06E+07
ZrD_2	5.60	5.72	104,000	1405	8.53E+06
YD_2	4.29	4.39	137,000	1871	8.94E+06
ScD_2	2.99	3.11	119,000	1507	9.67E+06
ErD_2	8.25	8.35	117,000	1724	8.49E+06

Fig. 5 is a sketch of a typical experimental setup for RPI's two-crystal system. One type of experiments done at RPI used tungsten nanorods in lieu of the copper disk and tip system typically used to collect charge from the crystal surface and locally enhance the electric field. During these experiments, ablation from the tungsten nanorod-coated crystal deposited onto the deuterated plastic target [5]. Fig. 6 is a picture of the target crystal after 20 experiments using W nanorods.

After experiments, the deuterated polyethylene target material often shows a discharge pattern on it which may be caused by charged particles skipping across the crystal surface. Fig. 6 shows that the tracks resulting from this particular set of experiments were coated with W from ablated material off the opposing crystal surface as indicated by the darker material present. Energy dispersive spectroscopy (EDS) confirmed the presence of W at these locations. Another interesting observation was that the discharge patterns in the plastic are near the outer edge of the crystal surface which is to be expected since the charge on the surface migrates toward that area of the crystal face [18].

The picture in Fig. 6 was analyzed using a software program (Gimp ver. 2.6) to estimate the amount of damage to the deuterated plastic target on the crystal surface. In this analysis, it was assumed that the darker area where the W was deposited was the extent of the target damage. By counting the darker colored pixels and comparing them to the total number of pixels in the target surface area, the amount of damage to the target was estimated to be 9.4% (±0.5%).

Scanning electron microscope (SEM) pictures were also taken of the target crystal surface before and after experiments to investigate the nature of the target erosion. Fig. 7 provides before and after pictures of the CD_2 target.

Fig. 7A shows raised tracks of plastic which appear to be seams resulting from the way the material was deposited (the plastic is melted and dropped onto the crystal surface using a glass pipette). Fig. 7B shows the crystal face after 20 experiments and a portion of the plastic that has apparently been torn away from the surface. This result may indicate the electric field was stronger near either the raised plastic tracks or the bare crystal surface due to tears in the polyethylene. The W material preferentially deposited in these areas due to the presence of a relatively higher electric field.

Another observation from the target crystal shown in Fig. 6 was that a surface crack in the $LiTaO_3$ occurred during the conduct of the experiments. Surface cracks of this nature may be caused by a spontaneous partial discharge of the crystal due to an electric arc to the chamber wall or other grounded materials nearby. Partial discharges from the crystal surface have been observed using a low light camera at RPI.

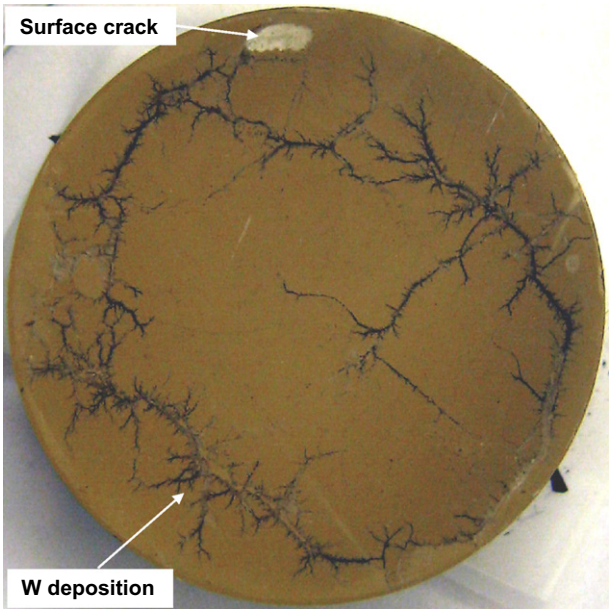

Fig. 6. Picture of W deposition on a 30 mm diameter crystal coated with CD_2 after 20 experiments using nanorods.

The picture in Fig. 7B was analyzed along with five other pictures to quantify the average width of the damage tracks. This analysis yielded an average width of the damage tracks of 120 (±20) μm. The maximum depth of the damage tracks appears from the SEM pictures to be the thickness of the target material. The thickness of the target material was measured using a profilometer to have an average thickness 4.2 (±0.7) μm.

While the calculations show the deuterated polyethylene target is superior to metal targets in terms of theoretical neutron yield, there may be advantages to using a metal target. For example, a metal target may be more robust in terms of target erosion. The pyroelectric crystal is heated to around 130 °C which may thermally degrade the plastic target. Also, it has been shown above that deuterated plastic becomes degraded over the course of experiments. Because the plastic is mounted directly on the crystal face, the electric field generated by the pyroelectric effect on the crystal surface may also be degraded due to polarization charges from the plastic. Being a conductor, metal would not have the same polarization effect.

Refs. [20,21] used a deuterated erbium target which they obtained from Los Alamos National Laboratory (LANL). Later, Ref.

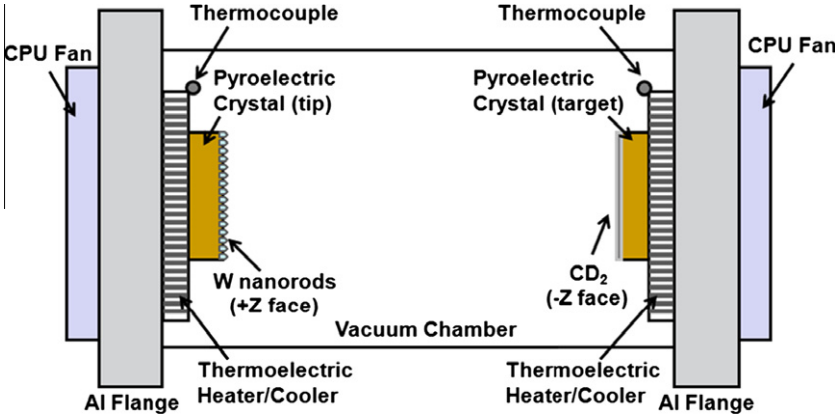

Fig. 5. Sketch of a typical two-crystal system at used for pyroelectric crystal fusion experiments at RPI.

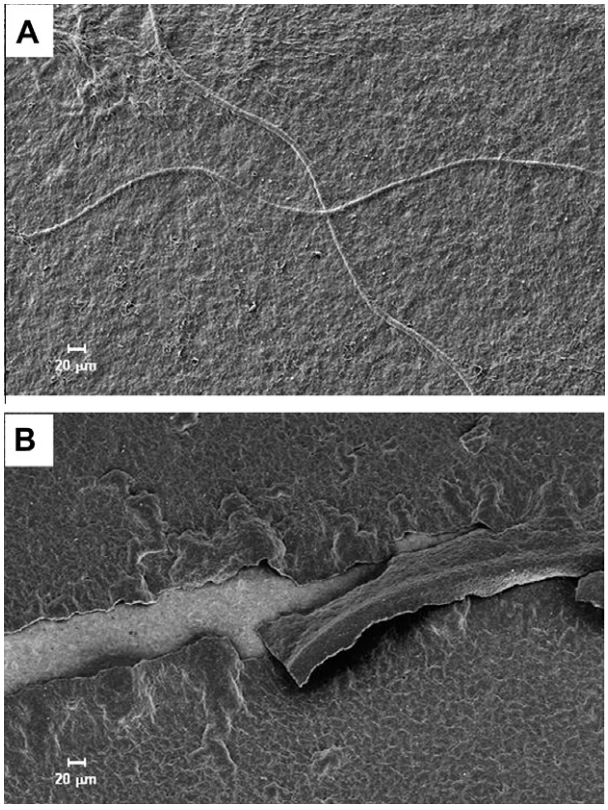

Fig. 7. SEM pictures of the target material deposited on the crystal face (A) before and (B) after 20 experiments [19].

[1] reported that they used a deuterated polystyrene target with a pulsed neutron generator [1].

The analysis presented in this paper shows that the best target material available for pyroelectric crystal fusion experiments in terms of the theoretical neutron yield is CD_2. Further experimental investigations using different metal targets are necessary to compare differences between plastic and metal targets in pyroelectric crystal fusion experiments.

4. Disclaimer

The views expressed herein are those of the author and do not reflect the position of the United States Military Academy, the Department of the Army, or the Department of Defense.

References

[1] V. Tang et al., J. Appl. Phys. 105 (2009) 026103.
[2] J. Geuther, Y. Danon, F. Saglime, Phys. Rev. Lett. 96 (2006) 054803.
[3] J.A. Geuther, Y. Danon, Appl. Phys. Lett. 90 (2007) 174103.
[4] D. Gillich, A. Kovanen, B. Herman, T. Fullem, Y. Danon, Nucl. Instrum. Method A 602 (2) (2009) 306–310.
[5] D.J. Gillich, R. Teki, T.Z. Fullem, A. Kovanen, E. Blain, D.B. Chrisey, T-M. Lu, Y. Danon, Nano Today 4 (3) (2009) 227–234.
[6] S.B. Lang, Phys. Today (August) (2005) 31–36.
[7] J.A. Geuther, Y. Danon, J. Appl. Phys. 97 (2005) 104916.
[8] M.B. Chadwick, P. Oblozinsky, M. Herman, et al., Nucl. Data Sheet 107 (2006) 2931–3060.
[9] J. Ziegler, M. Ziegler, Particle Interactions With Matter Web Page. <http://www.srim.org> (SRIM, Ver. 2008.05).
[10] S. Glasstone, R.H. Lovberg, Controlled Thermonuclear Reactions, D. Van Nostrand Company, Inc., New York, 1960.
[11] CRC Handbook of Chemistry and Physics, 89th ed., Taylor and Francis Group, LLC, 2009. <http://www.hbcpnetbase.com/>.
[12] C.E. Lundin, J.P. Blackledge, J. Electrochem. Soc. 109 (9) (1962) 838–841.
[13] E.A. St John, Solid Tritium and Deuterium Targets for Neutron Generators, US Patent 3320422, 16 May, 1967.
[14] C. Monnin, A. Ballanger, E. Sciora, A. Steinbrunn, P. Alexandre, G. Pelcot, Nucl. Instrum. Methods A 453 (2000) 493–500.
[15] J. Csikai, CRC Handbook of Fast Neutron Generators, vol. I, CRC Press, Boca Raton, Florida, 1987.
[16] G. Majer, J. Gottwald, U. Kaess, D.T. Peterson, R.G. Barnes, Phys. Rev. B 68 (2003) 134304.
[17] S.S. Sifhu, L. Heaton, D.D. Zauberis, Acta Cryst. 9 (1955) 607–614.
[18] N. Kukhtarev, J.T.D. Kukhtareva, M. Bayssie, J. Wang, J.D. Brownridge, J. Appl. Phys. 96 (11) (2004) 6794–6798.
[19] D.J. Gillich, Particle Acceleration with Pyroelectric Crystals, Ph.D. Dissertation, Rensselaer Polytechnic Institute, 2009, p. 122.
[20] B. Naranjo, J. Gimzewski, S. Putterman, Nature 434 (2005) 1115–1117.
[21] V. Tang et al., Rev. Sci. Instrum. 78 (12) (2007).